Koteswara Rao et al./ IJAIR Vol. 2 Issue 7 ISSN: 2278-7844

Image Segmentation in the Presence of Mixed Intensities with Application to MRI

N.Koteswara Rao[1] , J.V.K.Ratnam[2] , Y.muralikrishna[3]

[1] *Department of electronics and communication engineering, Narasaraopet Engineering College, Guntur, Ap, India*

[2]*Professor Department of electronics and communication engineering, Narasaraopet Engineering College, Guntur, Ap, India*

[3]*Assistant Professor Department of electronics and communication engineering, Narasaraopet Engineering College, Guntur, Ap, India*

Abstract— **Intensity inhomogeneity often occurs in real-world images, which presents a considerable challenge in image segmentation. The most widely used image segmentation algorithms are region-based and typically rely on the homogeneity of the image intensities in the regions of interest, which often fail to provide accurate segmentation results due to the intensity inhomogeneity. This paper proposes a novel region-based method for image segmentation, which is able to deal with intensity inhomogeneities in the segmentation. First, based on the model of images with intensity inhomogeneities, we derive a local intensity clustering property of the image intensities, and define a local clustering criterion function for the image intensities in a neighborhood of each point. This local clustering criterion function is then integrated with respect to the neighborhood center to give a global criterion of image segmentation. In a level set formulation, this criterion defines an energy in terms of the level set functions that represent a partition of the image domain and a bias field that accounts for the intensity inhomogeneity of the image. Therefore, by minimizing this energy, our method is able to simultaneously segment the image and estimate the bias field, and the estimated bias field can be used for intensity inhomogeneity correction (or bias correction). Our method has been validated on synthetic images and real images of various modalities, with desirable performance in the presence of intensity inhomogeneities. Experiments show that our method is more robust to initialization, faster and more accurate than the well-known piecewise smooth model. As an application, our method has been used for segmentation and bias correction of magnetic resonance (MR) images with promising results.**

KEYWORDSBias correction, image segmentation, intensity inhomogeneity, level set, MRI.

I. INTRODUCTION

Intensity inhomogeneity often occurs in real-world imagesdue to various factors, such as spatial variations in illumination and imperfections of imaging devices, which com plicates many problems in image processing and computer vision.

In particular, image segmentation may be considerably difficult for images with intensity inhomogeneities due to the overlaps between the ranges of the intensities in the regions to segmented. This makes it impossible to identify these regions based on the pixel intensity. Those widely used image segmentation algorithms [4], [17], [18], [23] usually rely on intensity homogeneity, and therefore are not applicable to images with intensity inhomogeneities. In general, intensity inhomogeneity has been a challenging difficulty in image segmentation. The level set method, originally used as numerical technique for tracking interfaces and shapes [14], has been increasingly applied to image segmentation in the past decade [2], [4], [5], [8]–[12], [15]. In the level set method, contours or surfaces are represented as the zero level set of a higher dimensional function, usually called a *level set function.* With the level set representation, the image segmentation problem can be formulated and solved in a principled way based on well-established mathematical theories, including calculus of variations and partial differential equations (PDE). An advantage of the level set method is that

numerical computations involving curves and surfaces can be performed on a fixed Cartesian grid without having to parameterize these objects. Moreover, the level set method is able to represent contours/surfaces with complex topology and change their topology in a natural way. Existing level set methods for image segmentation can be categorized into two major classes: *region-based models* [4], [10], [17], [18], [20], [22] and *edge-based models* [3], [7], [8], [12], [21]. Region-based models aim to identify each region of interest by using a certain region descriptor to guide the motion of the active contour. However, it is very difficult to define a region descriptor for images with intensity inhomogeneities. Most of region-based models [4], [16]–[18] are based on the assumption of intensity homogeneity. A typical example is *piecewise constant (PC) models* proposed in [4], [16]–[18]. In [20], [22], level set methods are proposed based on a general *piecewise smooth (PS)* formulation originally proposed by Mumford and Shah [13]. These methods do not assume homogeneity of image intensities, and therefore are able to segment images with intensity inhomogeneities. However, these methods are computationally too expensive and are quite sensitive to the initialization of the contour [10], which greatly limits their utilities. Edge-based models use edge information for image segmentation. These models do not assume homogeneity of image intensities, and thus can be applied to images with intensity inhomogeneities. However, this type of methods are in general quite sensitive to the initial conditions and often suffer from serious boundary leakage problems in images with weak object boundaries.

In this paper, we propose a novel region-based method for image segmentation. From a generally accepted model of images with intensity inhomogeneities, we derive a local intensity clustering property, and therefore define a local clustering criterion function for the intensities in a neighborhood of each point. This local clustering criterion is integrated over the neighborhood center to define an energy functional, which is converted to a level set formulation. Minimization of this energy is achieved by an interleaved process of level set evolution and estimation of the bias field. As an important application, our method can be used for segmentation and bias correction of magnetic resonance (MR) images. Note that this paper is an extended version of our preliminary work presented in our conference paper [9].

VARIATIONAL FRAMEWORK FOR JOINT SEGMENTATION AND BIAS FIELD ESTIMATION

A. Image Model and Problem Formulation

In order to deal with intensity inhomogeneities in image segmentation, we formulate our method based on an image model that describes the composition of real-world images, in which intensity inhomogeneity is attributed to a component of an image. In this paper, we consider the following multiplicative model of intensity inhomogeneity. From the physics of imaging in a variety of modalities (e.g. camera and MRI), an observed image I can be modeled as

$$I=bJ+n$$

Where J is the true image, b is the component that accounts for the intensity inhomogeneity, and is additive noise. The component is referred to as a *bias field* (or *shading image*). The true image J measures an intrinsic physical property of the objects being imaged, which is therefore assumed to be piecewise (approximately) constant. The bias field b is assumed to be slowly varying. The additive noise can be assumed to be zero-mean Gaussian noise.

In this paper, we consider the image I as a function defined on a continuous domain . The assumptions about the true image and the bias field can be stated more specifically as follows:

(A1) The bias field is slowly varying, which implies that can be well approximated by a constant in a neighborhood of each point in the image domain.

(A2) The true image J approximately takes N distinct constant values $C_1,\ldots C_N$ in disjoint regions $\Omega_1,\ldots\Omega_N$, respectively,where forms a *partition* of the imagedomain, i.e. and forbased on the model in (3) and the assumptions A1 and A2,we propose a method to estimate the regions , the constants, and the bias field . The obtained estimates ofthem are denoted by , the constants , and thebias field , respectively. The

obtained bias field should beslowly varying and the regions should satisfy certain regularity property to avoid spurious segmentation results caused by image noise. We will define a criterion for seeking such estimates based on the above image model and assumptions A1 and A2. This criterion will be defined in terms of the regions , constants , and function , as an energy in a variational framework, which is minimized for finding the optimal regions , constants , and bias field . As a result, image segmentation and bias field estimation are simultaneously accomplished.

B Local Intensity Clustering Property

Region-based image segmentation methods typically relies on a specific region descriptor (e.g. intensity mean or a Gaussian distribution) of the intensities in each region to be segmented. However, it is difficult to give such a region descriptor for images with intensity inhomogeneities. Moreover, intensity inhomogeneities often lead to overlap between the distributions of the intensities in the regions $\Omega_1,\ldots\Omega_N$. Therefore, it is impossible to segment these regions directly based on the pixel intensities. Nevertheless, the property of local intensities is simple, which can be effectively exploited in the formulation of our method for image segmentation with simultaneous estimation of the bias field.

based on the image model in (3) and the assumptions A1 and A2, we are able to derive a useful property of local intensities, which is referred to as a local intensity clustering property as described and justified below. To be specific, we consider a circular neighborhood with a radius ρ centered at each point $\mathbf{y} \in \Omega$, defined by $\mathcal{O}_{\mathbf{y}} \triangleq \{\mathbf{x} : |\mathbf{x}-\mathbf{y}| \leq \rho\}$. The partition $\{\Omega_i\}_{i=1}^N$ of the entire domain induces a partition of the neighborhood , i.e., $\{\mathcal{O}_{\mathbf{y}} \cap \Omega_i\}_{i=1}^N$ forms a partition of . For a slowly varying bias field b , the values b(x) for all x in the circular neighborhood are close to , i.e.

$$b(\mathbf{x}) \approx b(\mathbf{y}) \quad \text{for} \quad \mathbf{x} \in \mathcal{O}_{\mathbf{y}}$$

Thus, the intensities b(x)J(x) in each subregion $\mathcal{O}_{\mathbf{y}} \cap \Omega_i$ are close to the constantb(y)C_i , i.e.

$$b(\mathbf{x})J(\mathbf{x}) \approx b(\mathbf{y})c_i \quad \text{for} \quad \mathbf{x} \in \mathcal{O}_{\mathbf{y}} \cap \Omega_i$$

Then, in view of the image model in (3), we have

$$I(\mathbf{x}) \approx b(\mathbf{y})c_i + n(\mathbf{x}) \quad \text{for} \quad \mathbf{x} \in \mathcal{O}_{\mathbf{y}} \cap \Omega_i$$

where n(x) is additive zero-mean Gaussian noise. Therefore,the intensities in the set

$$\mathbf{I}_{\mathbf{y}}^i = \{I(\mathbf{x}) : \mathbf{x} \in \mathcal{O}_{\mathbf{y}} \cap \Omega_i\}$$

form a cluster with cluster center , which can be considered as samples drawn from a Gaussian distribution with mean . Obviously, the N clusters , are well-separated, with distinct cluster centers , (because the constants are distinct and the variance of the Gaussian noise is assumed to be relatively small). This local intensity clustering property is used to formulate the proposed method for image segmentation and bias field estimation as follows.

Energy Formulation

The above described local intensity clustering property indicates that the intensities in the neighborhood O_y can be classified into N clusters, with centers $m_i \approx b(y)_{Ci}$,i=1….N This allows us to apply the standard K-means clustering to classify these local intensities. Specifically, for the intensities I(x) in the neighborhood O_y , the K-means algorithm is an iterative process to minimize the clustering criterion [19], which can be written in a continuous form as

$$F_{\mathbf{y}} = \sum_{i=1}^{N} \int_{\mathcal{O}_{\mathbf{y}}} |I(\mathbf{x}) - m_i|^2 u_i(\mathbf{x}) d\mathbf{x}$$

Where m_i is the cluster center of the i -th cluster, $\mu_i(x)=1$ is the membership function of the region to be determined Since is the membership function of the region , we can rewrite as

$$F_{\mathbf{y}} = \sum_{i=1}^{N} \int_{\Omega_i \cap \mathcal{O}_{\mathbf{y}}} |I(\mathbf{x}) - m_i|^2 d\mathbf{x}.$$

In view of the clustering criterion in (7) and the approximation of the cluster center by , we define a clustering criterion for classifying the intensities in as

$$\mathcal{E}_{\mathbf{y}} = \sum_{i=1}^{N} \int_{\Omega_i \cap \mathcal{O}_{\mathbf{y}}} K(\mathbf{y}-\mathbf{x}) \, |I(\mathbf{x}) - b(\mathbf{y})c_i|^2 \, d\mathbf{x}$$

where K(y-x) is introduced as a nonnegative window function, also called kernel function, such that K(y-x)=0.With the window function, the clustering criterion function can be rewritten as

$$\mathcal{E}_{\mathbf{y}} = \sum_{i=1}^{N} \int_{\Omega_i} K(\mathbf{y}-\mathbf{x}) \, |I(\mathbf{x}) - b(\mathbf{y})c_i|^2 \, d\mathbf{x}.$$

This local clustering criterion function is a basic element in the formulation of our method.

EXPERIMENTAL RESULTS

We first demonstrate our method in the two-phase case (i.e N=2). Unless otherwise specified, the parameter is set to 4 for the experiments in this section. All the other parameters are set to the default values mentioned above Fig. 1 shows the results for a camera image of limon and a computed tomography angiography (CTA) image of blood vessel. The curve evolution processes are depicted by showing the initial contours (in the left column), intermediate contours (in the middle column),

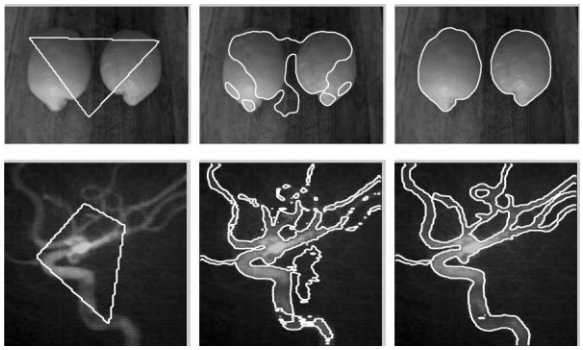

Fig. 1. Segmentation for an image of limon (upper row) and a CT image of vessel (lower row). The left, middle, and right columns show the initial contours (a triangle for the limon image and a quadrangle for the vessel image), the intermediate contours, and the final contours, respectively.

and the final contours (in the right column) on the images. Intensity inhomogeneities can be clearly seen in these two images. Our method is able to provide a desirable segmentation result for such images. The estimated bias field by our method can be used for intensity inhomogeneity correction (or bias correction). Given the estimated bias field , the bias corrected image is computed as the quotient . To demonstrate the effectiveness of our method in simultaneous segmentation and bias field estimation, we applied it to three medical images with intensity inhomogeneities: an MR image of breast, an X-ray image of bones, and an ultrasound image of prostate. These images exhibit obvious intensity inhomogeneities. The ultrasound image is also corrupted with serious speckle noise.We applied a convolution with a Gaussian kernel to smooth the ultrasound image as a preprocessing step. The scale parameter of the Gaussian kernel is chosen as 2.0 for smoothing this ultrasound image. The initial contours are plotted on the original images in Column 1 of Fig. 2. The corresponding results of segmentation, bias field estimation, and bias correction are shown in Columns 2, 3, and 4, respectively. These results demonstrate desirable performance of our method in segmentation and bias correction.

A. Performance Evaluation and Method Comparison

As a level set method, our method provides a contour as the segmentation result. Therefore, we use the following contour- based metric for precise evaluation of the segmentation result. Let C be a contour as a segmentation result, and S be the true object boundary, which is also given as a contour. For each point p, i=1….N on the contour , we can compute the distance from the point Pi to the ground truth contour , denoted by . Then, we define the deviation from the contour C to the ground truth S by

$$e_{\text{mean}}(C) = \frac{1}{N} \sum_{i=1}^{N} \text{dist}(P_i, S)$$

which is referred to as the mean error of the contour C . This contour-based metric can be used to evaluate a subpixel accuracy of a segmentation result given by a contour.

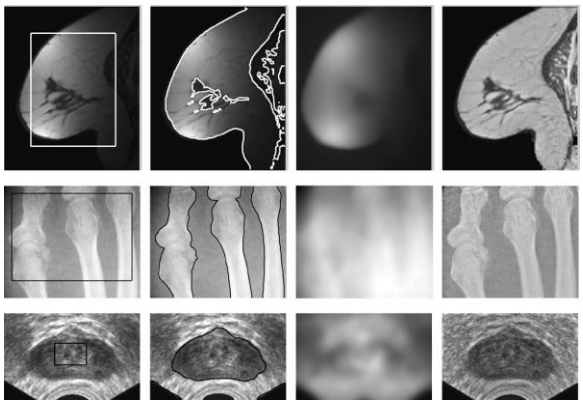

Fig. 2. Applications of our method to an MR image of breast, an X-ray image of bones, and an ultrasound image of prostate. Column 1: Initial contour on the original image; Column 2: Final contours; Column 3: Estimated bias field; Column 4: Bias corrected image.

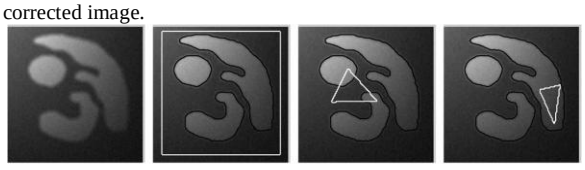

(a) (b) (c) (d)

Fig. 3. Robustness of our method to contour initializations is demonstrated by its results for an synthetic image in (a) with different initial contours. The initial contours (white contours) and corresponding segmentation results (black contours) are shown in (b–d).

1) Robustness to Contour Initialization: With the above metrics, we are able to quantitatively evaluate the performance of our method with different initializations and different settings of parameters. We applied our method to a synthetic image in Fig. 3 with 20 different initializations of the contour and the constants. For examples, we show three of the 20 initial contours (white contours) and the corresponding results (black contours) in Fig. 3. In these three different initializations, the initial contour encloses the objects of interest [in Fig. 3(b)], crosses the objects [in Fig. 3(c)], and totally inside of one object [in Fig. 3(d)]. Despite the great difference of these initial contours, the corresponding results are almost the same, all accurately capturing the object boundaries. The segmentation accuracy is quantitatively verified by evaluating these results in terms of mean errors. The mean errors of these results are all between 0.21 and 0.24 pixel, as shown in Fig. 4(a). These experiments demonstrate the robustness of our model to contour initialization and a desirable accuracy at subpixel level.

2) Stable Performance for Different Scale Parameters: We also tested the performance of our method with different scale parameters , which is the most important parameter in our model. For this image, we applied our method with 12 different values of from 4 to 15. The corresponding mean errors of these 12 results are plotted in Fig. 4(b). While the mean error increases as increases, it is below 0.5 pixel for all the 12 different values of used in this experiment.

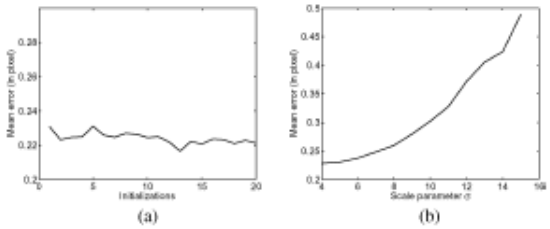

(a) (b)

Fig. 4. Segmentation accuracy of our method for different initializations and different scale parameters σ. (a) Mean errors of the results for 20 different initializations;
(b) Mean errors of the results for 12 different scale parameters σ with $\sigma = 4, 5, 6 \ldots \ldots \ldots$

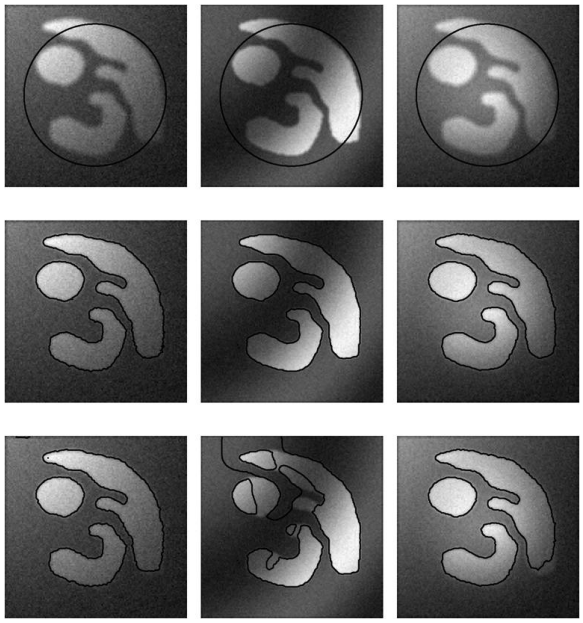

Fig. 5. Performances of our method and the PS model in different imageconditions (e.g. different noise, intensity inhomogeneities, and weak object boundaries). Top row: Initial contours plotted on the original image; Middle row: Results of our method; Bottom row: Results of the PS model.

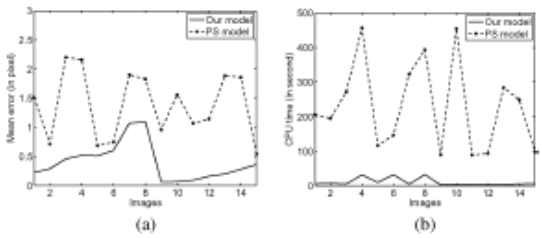

(a) (b)

Fig. 6. Comparison of our model and the PS model in terms of accuracy and CPU time. (a) Mean errors. (b) CPU times.

Comparison With Piecewise Smooth Model

We can also quantitatively compare our method with the PS model on synthetic images. We generated 15 different images with the same objects, whose boundaries are known and used as the ground truth. These 15 images are generated by smoothing an ideal binary image, adding intensity inhomogeneities of different profiles and different levels of noise. Fig. 5 show three of these images as examples, with the corresponding results of our model and the PS model in the middle and bottom rows, respectively. We use the same initial contour (the circles in the top

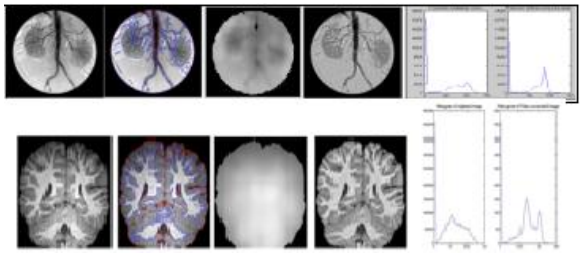

Fig. 7. Applications of our method to 3T MR images. Column 1: Original image; Column 2: Final zero level contours of $\sigma 1$ (red) and $\sigma 2$ (blue), i.e. the segmentation result; Column 3: Estimated bias fields; Column 4: Bias corrected images; Column 5: Histograms of the original images (left) and bias corrected images (right).

row) for the two models and all the 15 images. It is obvious that our model produces more accurate segmentation results than the PS model. To quantitatively evaluate the accuracy, we compute the mean errors of both models for all the 15 images, which are plotted in Fig. 6(a), where the -axes represent 15 different images. As shown in Fig. 6(a), the errors of our model are significantly lower than those of the PS model. On the other hand, our model is much more efficient than the PS model. This can be seen from the CPU times consumed by the two models for the 15 images [see Fig. 6(b)]. In this experiment, our model is remarkably faster than the PS model, with an average speed-up factor 36.43 in our implementation. The CPU times in this experiment were recorded in running our Matlab programs on a Lenovo ThinkPad notebook with Intel (R) Core (TM)2 Duo CPU, 2.40 GHz, 2 GB RAM, with Matlab 7.4 on Windows Vista. *C. Application to MR Image Segmentation and Bias Correction* In this subsection, we focus on the application of the proposed method to segmentation and bias correction of brain MR images. We first show the results for 3T MR images in the first column of Fig. 7. These images exhibit obvious intensity inhomogeneities. The segmentation results, computed bias fields, bias corrected images, are shown in the second, third, and fourth column respectively. It can be seen that the intensities within each tissue become quite homogeneous in the bias corrected images. The improvement of the image quality in terms of intensity homogeneity can be also demonstrated by comparing the histograms of the original images and the bias corrected images. The histograms of the original images (left) and the bias corrected images (right) are plotted in the fifth column. There are three well-defined and well-separated peaks in the histograms of the bias corrected image, each corresponding to a tissue or the background in the image. In contrast, the histograms of the

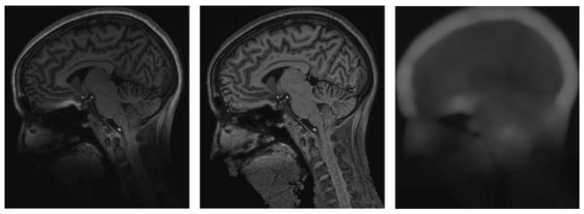

(a) (b) (c)

Fig. 8. Application to a 7T MR image. (a) Original image; (b) Bias corrected image; (c) Computed bias field.

original images do not have such well-separated peaks due to the mixture of the intensity distribution caused by the bias. Our method has also been tested on 7T MR images with promising results. At 7T, significant gains in image resolution can be obtained due to the increase in signal-to-noise ratio. However, susceptibility-induced gradients scale with the main field, while the imaging gradients are currently limited to essentially the same strengths as used at lower field strengths (i.e., 3T). Such effects are most pronounced at air/tissue interfaces, as can be seen at the base of the frontal lobe in Fig. 8(a). This appears as a highly localized and strong bias, which is challenging to traditional methods for bias correction. The result for this image shows the ability of our method to correct such bias, as shown in Fig. 8(b) and (c).

CONCLUSION

We have presented a variational level set framework for segmentation and bias correction of images with intensity inhomogeneities. Based on a generally accepted model of images with intensity inhomogeneities and a derived local intensity clustering property, we define an energy of the level set functions that represent a partition of the image domain and a bias field that accounts for the intensity inhomogeneity. Segmentation and bias field estimation are therefore jointly performed by minimizing the proposed energy functional. The slowly varying property of the bias field derived from

the proposed energy is naturally ensured by the data term in our variational framework, without the need to impose an explicit smoothing term on the bias field. Our method is much more robust to initialization than the piecewise smooth model. Experimental results have demonstrated superior performance of our method in terms of accuracy, efficiency, and robustness.

REFERENCES

[1] G. Aubert and P. Kornprobst, *Mathematical Problems in Image Processing: Partial Differential Equations and the Calculus of Variations*.New York: Springer-Verlag, 2002.

[2] V. Caselles, F. Catte, T. Coll, and F. Dibos, "A geometric model for active contours in image processing," *Numer. Math.*, vol. 66, no. 1, pp.1–31, Dec. 1993.

[3] V. Caselles, R. Kimmel, and G. Sapiro, "Geodesic active contours,"*Int. J. Comput. Vis.*, vol. 22, no. 1, pp. 61–79, Feb. 1997.

[4] T. Chan and L. Vese, "Active contours without edges," *IEEE Trans.Image. Process.*, vol. 10, no. 2, pp. 266–277, Feb. 2001.

[5] D. Cremers, "A multiphase levelset framework for variational motion segmentation," in *Proc. Scale Space Meth. Comput. Vis.*, Isle of Skye,U.K., Jun. 2003, pp. 599–614.

[6] L. Evans, *Partial Differential Equations*. Providence, RI: Amer.Math. Soc., 1998.

[7] S. Kichenassamy, A. Kumar, P. Olver, A. Tannenbaum, and A. Yezzi,"Gradient flows and geometric active contour models," in *Proc. 5th Int.Conf. Comput. Vis.*, 1995, pp. 810–815.

[8] R. Kimmel, A. Amir, and A. Bruckstein, "Finding shortest paths on surfaces using level set propagation," *IEEE Trans. Pattern Anal. Mach. Intell.*, vol. 17, no. 6, pp. 635–640, Jun. 1995.

[9] C. Li, R. Huang, Z. Ding, C. Gatenby, D. Metaxas, and J. Gore, "A variational level set approach to segmentation and bias correction of medical images with intensity inhomogeneity," in *Proc. Med. Image Comput. Comput. Aided Intervention*, 2008, vol. LNCS 5242, pp. 1083–1091, Part II.

[10] C. Li, C. Kao, J. C. Gore, and Z. Ding, "Minimization of region-scalable fitting energy for image segmentation," *IEEE Trans. Image Process.*, vol. 17, no. 10, pp. 1940–1949, Oct. 2008.

[11] C. Li, C. Xu, C. Gui, and M. D. Fox, "Distance regularized level set evolution and its application to image segmentation," *IEEE Trans. Image Process.*, vol. 19, no. 12, pp. 3243–3254, Dec. 2010.

[12] R. Malladi, J. A. Sethian, and B. C.Vemuri, "Shape modeling with front propagation: A level set approach," *IEEE Trans. Pattern Anal. Mach.Intell.*, vol. 17, no. 2, pp. 158–175, Feb. 1995.

[13] D. Mumford and J. Shah, "Optimal approximations by piecewise smooth functions and associated variational problems," *Commun.Pure Appl. Math.*, vol. 42, no. 5, pp. 577–685, 1989.

[14] S. Osher and J. Sethian, "Fronts propagating with curvature-dependent speed: Algorithms based on Hamilton-Jacobi formulations," *J. Comp.Phys.*, vol. 79, no. 1, pp. 12–49, Nov. 1988.

[15] N. Paragios and R. Deriche, "Geodesic active contours and level sets for detection and tracking of moving objects," *IEEE Trans. Pattern Anal.Mach. Intell.*, vol. 22, no. 3, pp. 266–280, Mar. 2000.

[16] N. Paragios and R. Deriche, "Geodesic active regions and level set methods for supervised texture segmentation," *Int. J. Comput. Vis.*, vol. 46, no. 3, pp. 223–247, Feb. 2002.

[17] R. Ronfard, "Region-based strategies for active contour models," *Int.J. Comput. Vis.*, vol. 13, no. 2, pp. 229–251, Oct. 1994.

[18] C. Samson, L. Blanc-Feraud, G. Aubert, and J. Zerubia, "A variational model for image classification and restoration," *IEEE Trans. Pattern Anal. Mach. Intell.*, vol. 22, no. 5, pp. 460–472, May 2000.

[19] S. Theodoridis and K.Koutroumbas, *Pattern Recognition*. NewYork: Academic, 2003.

[20] A. Tsai, A. Yezzi, and A. S.Willsky, "Curve evolution implementation of the Mumford-Shah functional for image segmentation, denoising, interpolation, and magnification," *IEEE Trans. Image Process.*, vol. 10, no. 8, pp. 1169–1186, Aug. 2001.

[21] A. Vasilevskiy and K. Siddiqi, "Flux-maximizing geometric flows," *IEEE Trans. Pattern Anal. Mach. Intell.*, vol. 24, no. 12, pp. 1565–1578, Dec. 2002.

[22] L. Vese and T. Chan, "A multiphase level set framework for image segmentation using the Mumford and Shah model," *Int. J. Comput. Vis.*, vol. 50, no. 3, pp. 271–293, Dec. 2002.

[23] S.-C. Zhu and A. Yuille, "Region competition: Unifying snakes, region growing, and Bayes/MDL for multiband image segmentation," *IEEE Trans. Pattern Anal. Mach. Intell.*, vol. 18, no. 9, pp. 884–900, Sep. 1996.maximum power point in photovoltaic systems," *IEEE Power Electron. Lett.*, vol. 2, no. 1, pp. 16–19, Mar. 2004.

[18] A. Pandey, N. Dasgupta, and A. K. Mukerjee, "Design issues in implementing MPPT for improved tracking and dynamic performance," in *Proc. 32nd IECON*, Nov. 2006, pp. 4387–4391.

[19] K. H. Hussein, I. Muta, T. Hoshino, and M. Osakada, "Maximum photovoltaic power tracking: An algorithm for rapidly changing atmospheric conditions," *Proc. Inst. Elect. Eng.—Gener., Transmiss. Distrib.*, vol. 142, no. 1, pp. 59–64, Jan. 1995.

[20] T.-F.Wu, C.-H. Chang, and Y.-H. Chen, "A fuzzy-logic-controlled singlestage converter for PV-powered lighting system applications," *IEEE Trans. Ind. Electron.*, vol. 47, no. 2, pp. 287–296, Apr. 2000.

[21] M. Veerachary, T. Senjyu, and K. Uezato, "Neural-network-based maximum-power-point tracking of coupled-inductor interleaved-boostconverter